Endocytosis caused by liquid-liquid phase separation of proteins

Louis-Philippe Bergeron-Sandoval[1], Hossein Khadivi Heris[2], Catherine Chang[3], Caitlin E. Cornell[3], Sarah L. Keller[3], Paul François[4], Adam G. Hendricks[2], Allen J. Ehrlicher[2], Rohit V. Pappu[5] and Stephen W. Michnick[1,6*]

Affiliations

[1]Département de Biochimie, Université de Montréal, C.P. 6128, Succursale centre-ville, Montréal, Québec, H3C 3J7, Canada.
[2]Department of Bioengineering, McGill University, 817 Sherbrooke St West, Room 270, Montreal, Quebec, H3A 0C3, Canada.
[3]Department of Chemistry, University of Washington, Seattle, Seattle WA 98195-1700 USA
[4]Ernest Rutherford Physics Building, McGill University, 3600 University St, Montreal, Québec, H3A 2T8
[5]Department of Biomedical Engineering and Center for Biological Systems Engineering, Washington University in St. Louis, One Brookings Drive, Campus Box 1097, St. Louis, Missouri 63130, USA.
[6]Centre Robert-Cedergren, Bio-Informatique et Génomique, Université de Montréal, C.P. 6128, Succursale centre-ville, Montréal, Québec, H3C 3J7, Canada.

*Correspondence to: S.W.M. (stephen.michnick@umontreal.ca).

Summary

Endocytosis underlies intra- and extracellular material trafficking in eukaryotes, and is essential to protein metabolism, intercellular signaling, membrane remodeling and other cell regulatory processes. Although endocytosis is usually driven by F-actin polymerization in yeast cells, membrane invagination can also occur through a yet unknown actin-independent mechanism when turgor pressure is relieved. Here, we demonstrate that membrane invagination can arise from liquid-liquid phase separation (demixing) of proteins with prion-like domains (PLD) from the cytosol. Demixing of these proteins results in the formation of a protein condensate, which, by virtue of its composition and viscoelastic properties, binds to and deforms plasma membrane and cytosol. Demonstration that phase separated condensates can perform mechanical work expands the repertoire of known functions of protein condensates to include the ability to do work at soft interfaces such as between the condensate and the membrane. Similar mechanisms may govern or contribute to other membrane shaping, invagination and budding processes that are involved in cellular material uptake, secretion, and cell shape remodeling.

Introduction

Evolution has resulted in numerous innovations by which morphogenesis of organisms occurs within limits imposed by physical and chemical constraints (Darwin 1859, Thompson 1917). One such process is clathrin-mediated endocytosis (CME) a fundamental mechanism of cell surface membrane receptor turnover and recycling, nutrient uptake and synaptic vesicle regeneration, among others (Conner and Schmid 2003). The mechanism of membrane invagination through endocytosis in budding yeast cells has most convincingly been demonstrated to be growth of membrane-bound branched actin (Skruzny, Brach et al. 2012), although the term "CME" has historically been retained. When actin is polymerized, it bundles into an active gel with mechanical properties that facilitate endocytosis at localized sites (Carlsson and Bayly 2014, Weirich, Banerjee et al. 2017). However, CME has also been shown to occur under conditions where actin polymerization is absent in both yeast and mammalian cells (Aghamohammadzadeh and Ayscough 2009, Basu, Munteanu et al. 2014, Li, Shao et al. 2015).

The contribution of actin polymerization to CME in mammalian cells is ambiguous, since equal population of clathrin-coated pits mature into vesicles either with or without the need for cortical filamentous actin at endocytic sites (Li, Shao et al. 2015). In the budding yeast *S. cerevisiae,* the dominant mechanism for vesicle generation in CME is branched actin assembly, which is required to compete against intracellular turgor pressure and membrane tension to drive the invagination of the plasma membrane (Carlsson and Bayly 2014). If, however, turgor pressure is eliminated in yeast cells, CME can also occur, independent of actin polymerization (Aghamohammadzadeh and Ayscough 2009). A similar phenomenon has been observed in fission yeast (Basu, Munteanu et al. 2014). Several mechanisms that could explain actin-independent membrane invagination in CME have been proposed (see Discussion) but individual or combined contributions of these mechanisms to CME *in vivo* remain unclear.

Here, we present evidence for a novel mechanism of actin-independent CME in a yeast cell mutant model in which turgor pressure is relieved and actin polymerization is specifically inhibited (Figure 1A and S1). This mechanism was suggested to us by the observation that there is a common intrinsically disordered amino acid sequence pattern called prion-like domains (PLD) found among coat and adapter proteins Sla1/2, Ent1/2 and Yap1801/2 (Figure 1A) (Alberti, Halfmann et al. 2009, Malinovska, Kroschwald et al. 2013). PLD-containing proteins are known to phase separate *in vitro* and in cells and interact through amino acid sequence motifs found within the PLDs (Alberti, Saha et al. 2018, Wang, Choi et al. 2018). Phase separation leads to spherical condensates that are hundreds of nanometers to micrometers in size with a range of viscoelastic properties (Pappu, Wang et al. 2008, Brangwynne, Eckmann et al. 2009, Kroschwald, Maharana et al. 2015, Molliex, Temirov et al. 2015, Wang, Choi et al. 2018). Nucleation and growth of such condensates within cells has the potential to deform the cytosol and other elastic structures found inside these cells (Style, Sai et al. 2018). It has also been demonstrated that membranes can be deformed *in vitro* by liquid-liquid phase separation of polymer condensates (Li, Lipowsky et al. 2011).

We postulate that such condensates exist at CME initiation sites and that, owing to their viscoelastic properties and interfacial tension, bind to the plasma membrane adaptors and generate force to drive invagination of the membrane (Figure 1A). This model can implicitly include and integrate the contributions of the previously proposed mechanisms for membrane invagination in actin-independent CME (detailed in the Discussion). Notably, our model explains how proteins are concentrated at endocytic sites to bind to and alter the properties or composition of the membrane, such that elastic resistance of the membrane to deformation is reduced.

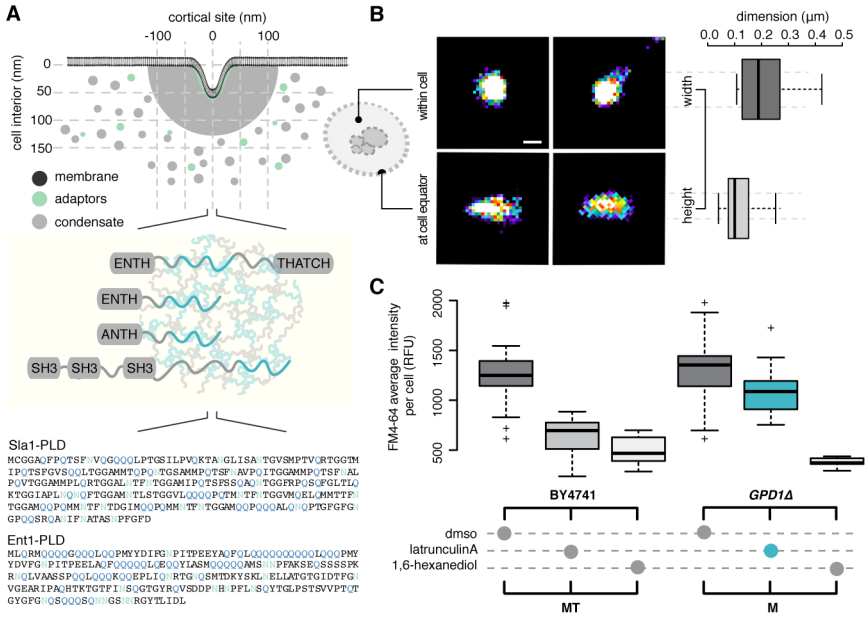

Figure 1 | Phase-separation of proteins into a endocytic condensate can drive clathrin-mediated endocytosis (A) (Upper panel) Illustration of the geometry of a plasma membrane (dark grey) invagination into the cell during clathrin-mediated endocytosis (CME). Electron microscopic data suggest that clathrin-coated plasma membrane patches are surrounded by a cortical body of ~200 nm diameter (light grey) before appearance of actin structures. Clathrin heavy and light chains (Chc1 and Clc1) interact with adaptor proteins (Ede1 and Syp1) to form a lattice on the membrane (in green). Subsequently, early coat proteins (light grey), such as Sla1/2, Ent1/2, and Yap1801/2, directly bind to the adaptor-clathrin lattice and form the endocytic condensate (in grey). (middle panel) Coat proteins Sla1/2, Ent1/2 and Yap1801/2 contain "Prion-like domains" (PLD, in blue) that include tandem repeats of asparagine and glutamine. (lower panel) Examples of PLD sequences from Sla1 and Ent1 (B) Geometry and size distribution of coat protein Sla1-GFP at cortical sites measured using super-resolution microscopy (dSTORM). Lateral x, y resolution was ~10 nm. Pseudo-color reconstructed images show circular structures (left panels) when viewed from the top, or within cells (left, upper), but form narrow ellipses when imaged at the equator of cells (left, lower). Automatic segmentation and morphological analysis (right panels) were performed on these reconstructed images to determine the width (209 ± 10 nm) and height (118 ± 6 nm) of cortical bodies (mean ± sd; n = 250), consistent with other electron and light micrographic evidence. (C) Lipophilic cargo membrane-labelling dye FM4-64 is taken up into vesicles by CME in wild type BY4741 (left) and *GPD1*Δ cells (eliminates turgor pressure; right) treated with either DMSO, latrunculin A (prevents F-actin polymerization) or 1,6-hexanediol (disrupts liquid-liquid phase separated protein condensates). Each boxplot (center line, median; box, upper and lower quartiles; whiskers, 1.5x IQR; crosses, outliers) shows

the relative fluorescence units of n = 50 cells. Note that *GPD1*Δ cells can undergo CME in the absence of F-actin polymerization (blue) because there is no turgor pressure in these cells. See also Figure S1.

PLD-containing CME proteins phase-separate into protein condensates

We first observed protein puncta that form at cortical sites of 209 ± 10 nm diameter and 118 ± 6 nm height by super-resolution fluorescence imaging of the PLD-containing endocytic coat protein Sla1 in *GPD1*Δ cells treated with Latrunculin A (Lat A), an inhibitor of actin polymerization (Figure 1B and S1). Our data, which are similar to reported measures of Sla1 high resolution structures (Mund, van der Beek et al. 2017), indicate that Sla1 assembles into a dome-shaped structure under the conditions that we performed these experiments, consistent with a protein condensate (henceforth called the endocytic condensate) that associates with the membrane on cortical sites. Other existing evidence that a protein condensate could exist at CME sites include electron and light microscopic studies that reveal a region surrounding CME membrane invaginations of ~200 nm diameter that are devoid of ribosomes. Furthermore, before actin polymerization is initiated (as visualized by fluorescent protein-tagged Apb1) these "ribosome-free zones" are also observed on most sites (75%) suggesting that these zones can be composed of coat proteins (as visualized by fluorescent protein-tagged Sla1) and do not contain polymerized actin (Kukulski, Schorb et al. 2012). Sla1-labelled condensates thus appear to present a physical barrier to large molecular complexes, at least as large as ribosomes (> 25 nm). We next performed a series of experiments to establish that endocytic puncta are phase-separated protein condensates and we probed their properties and permeability.

The simple alcohol 1,6-hexanediol (HD) has been demonstrated to prevent liquid-liquid phase separation of proteins *in vivo* and *in vitro* (Updike, Hachey et al. 2011, Kroschwald, Maharana et al. 2015, Molliex, Temirov et al. 2015). CME, as measured by cell uptake of a lipophilic membrane-bound fluorescent dye (FM4-64), was inhibited by HD, whether or not turgor pressure and actin polymerization were present (Figure 1C, left *versus* right panels, respectively). Furthermore, HD prevented uptake of the fluorescent dye Lucifer Yellow (LY) into vacuoles and formation of puncta monitored as Sla1-GFP fluorescence at cortical sites in a dose-dependent manner. No effect was observed in cells treated with the related alcohol 1,2,3-hexanetriol that does not disrupt condensates (Figure 2A and S2A). The other PLD-containing proteins, including Sla2, Ent1, Ent2, Yap1801 and Yap1802, all failed to form puncta in cells treated with HD (Figure S2A). Pulse-chase experiments showed that HD-dependent dissolution of Sla1 puncta was reversible (Figure S2B and Movie S1). In controls, we found 5% HD has no major effect on the integrity of lipid vesicles containing carboxyfluorescein as an indicator of leakage (Figure S2C-E).

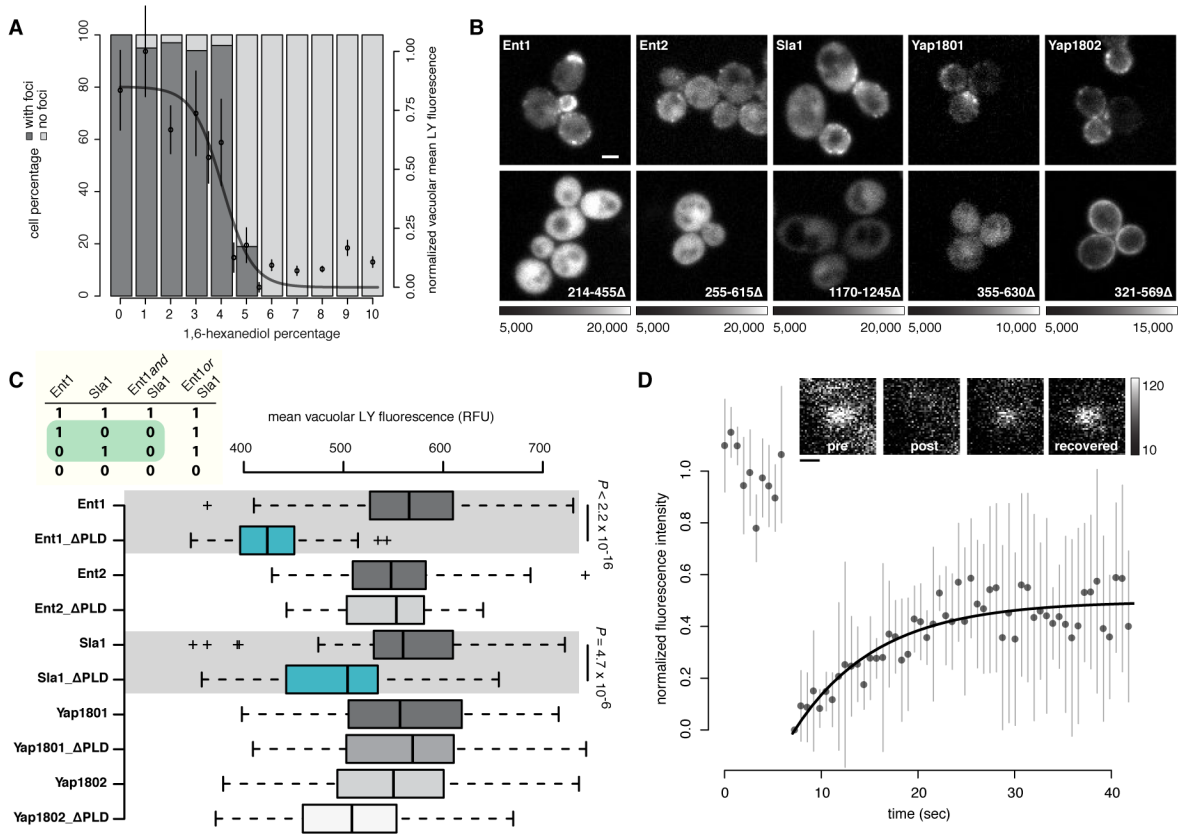

Figure 2 | CME adaptor and coat proteins phase separate to form condensates (A) 1,6-hexanediol (HD), disrupts endocytic condensates in an all-or-none manner. Barplot shows percentage of cells that contain Sla1-GFP foci (dark grey), or not (light grey), as a function of HD concentration monitored by counting fluorescent puncta containing Sla1-GFP at cortical sites 5 minutes after HD treatment (n = 150 cells). Plot overlay (in black) shows quantification of lucifer yellow fluorescent dye uptake in CME vesicles (mean ± sd; n = 25 foci; logistic fit) (B) Prion-like domains (PLDs) are essential for localization of proteins to the cortical sites. Fluorescence images of cortical localization of Ent1, Ent2, Sla1, Yap1801 and Yap1802 fused to Venus YFP. Localization of full-length (upper panels) *versus* C-terminal PLD truncation mutants of the proteins (lower panels). Amino acid positions of the deleted PLDs are indicated for respective images. Grayscale dynamic range for image pairs are indicated below. Scale bar, 2 μm. (C) Quantification (box center line, median; box limits, upper and lower quartiles; whiskers, 1.5x IQR; crosses, outliers) by fluorescence microscopy of lucifer yellow dye uptake for strains that express either full-length or PLD-truncated Ent1, Ent2, Yap1801, Yap1802 and Sla1 (as detailed in panel b). We observed a significant decrease in CME for PLD truncation mutants of Sla1 and Ent1 (n = 100 cells; two-sided t-test; see Methods). Presence (1) or absence (0) of the PLDs of either Ent1 or Sla1 are the input variables in the truth table (top insert; values that we determined in green). (D) Coat proteins exchange with endocytic condensates at rates typical of those observed for proteins that compose other protein condensates. Fluorescence recovery after photo bleaching (FRAP) of Sla2-GFP, GFP signal recovery was measured within a segmented Sla1-mCherry region of interest to ensure that FRAP was acquired within the endocytic condensate (mean ± sd; n = 10 cells. Data was fitted to a single term recovery equation) (Methods). Incomplete fluorescence recovery suggests that endocytic condensates are viscoelastic. Representative foci images before bleaching, upon bleaching, and after recovery are shown in inserts. 8-bit grayscale values, 10 to 120. Scale bar, 250 nm. See also Figure S2.

171 Alberti *et al*. reported that PLDs of Sla1/2, Ent1/2 and Yap1801/2 all form puncta individually,
172 without amyloid fibril structures, as probed by binding to Thioflavin T (ThT) (Khurana, Coleman
173 et al. 2005, Alberti, Halfmann et al. 2009). Consistent with the behavior of these PLD fragments
174 and formation of non-amyloid condensates, we observed no colocalization of ThT with Sla1-
175 mCherry-labelled puncta (Figure S2F-G).
176
177 We observed that the PLDs of CME coat proteins were essential to their localization to cortical
178 sites (Figure 2B). Furthermore, CME was significantly reduced in cells where the PLDs of Sla1
179 and Ent1 were deleted and with substitutions of proline for other residues in the Sla1 PLD, which
180 weakens the driving force for phase separation (Figure 2C and S2H) (Toombs, McCarty et al.
181 2009, Peskett, Rau et al. 2018). Our results are consistent with previous reports of the mis-
182 localization of the N-terminal SH3 domains of Sla1 (Warren, Andrews et al. 2002) and of the Ent2
183 ENTH2 domain (Mukherjee, Coon et al. 2009). They are also consistent with disruption of CME
184 resulting from deletion of the Sla1 C-terminal region (Warren, Andrews et al. 2002). While some
185 functional redundancy is possible among the PLD-containing coat proteins, the two that are most
186 essential, Sla1 and Ent1, are both required for specific protein-protein interactions and/or functions
187 mediated by other domains within their sequences.
188
189 The interactions among proteins in liquid-liquid phase separated condensates are expected to be
190 weak (Li, Chavali et al. 2018), explaining their rapid exchange within and between condensates
191 and their surroundings (Brangwynne, Eckmann et al. 2009, Lin, Protter et al. 2015, Feric, Vaidya
192 et al. 2016). In fluorescence recovery after photobleaching (FRAP) experiments we measured
193 equivalent mobile and immobile fractions (0.50 ± 0.02; mean ± sem) for the protein Sla2 (Figure
194 2E), similar to other protein and nucleic acid condensates including the dense internal fibrillar
195 component of *X. laevis* nucleoli (Feric, Vaidya et al. 2016). We acquired recovery traces when the
196 apparent number of Sla2 molecules in the fluorescent foci remains relatively constant (pre-bleach
197 intensities do not increase in Figure 2E).
198
199 **Condensation is required for CME protein-protein interactions and endocytosis**
200
201 The regulation of CME involves the dynamic assembly of a protein-protein interaction network
202 through mostly transient and weak protein-protein interactions (Boeke, Trautmann et al. 2014).
203 This observation begs a subtle and important question: Is the formation of the protein-protein
204 interaction network the result of phase separation into condensates or do endocytic condensates
205 reflect the formation of an obligate and fixed protein-protein interaction network? One could
206 argue, for instance, that deletion of the PLDs of Sla1 and Ent1 prevents membrane invagination
207 and therefore endocytosis by virtue of removal of binding motifs in the PLDs required for
208 interactions of both of these proteins (Figure 2B-C). It could even be argued that the subtle proline
209 substitution mutations in the Sla1 PLD inhibit CME because they prevent protein-protein

interactions by disrupting alpha-helical structural motifs essential for the protein-protein interactions of Sla1 (Figure S2H).

We distinguish these two possibilities based on simple logic as formally introduced in a truth table (Figure 3A, D): If the PLDs of Ent1 and Sla1 are *both* required for forming protein-protein interactions essential for CME then we *cannot* substitute the PLD of one for the other. If, however, we can substitute one PLD for the other and recover both phase separation and CME function, then the properties of the PLDs that allow them to phase-separate and allow for endocytosis is important rather than the fixed protein interaction network. A caveat would arise if Sla1 and Ent1 PLDs shared common binding motifs that govern essential protein-protein interactions. We found, however, that Sla1 PLD and Ent1 PLD share low sequence identity (23.6 percent) and the single motif TG(F/Y)GFGN (Figure S3A). More importantly, they share only two protein-protein interactions that are not essential to endocytosis (Chc1 and Ubi4; physical interactions detected by at least two experiments from the BioGRID database).

Since both Sla1 *and* Ent1 PLD domains are essential for endocytic condensate localization and endocytosis (Figure 2C), we needed to test the essentiality of the PLD of only one of these proteins and therefore chose that of Sla1. We first compared the protein-protein interactions between *wildtype* and the PLD deletion mutant of Sla1 *in vivo* using a Protein-fragment Complementation Assay with the reporter protein DiHydroFolate Reductase (DHFR PCA) (Figure S3B-C). We confirmed 13 potential Sla1 protein-protein interactions selected from *BioGRID* (thebiogrid.org) found amongst membrane adaptors (Chc1, Ede1, End3), PLD-containing coat proteins (Sla1, Sla2, Yap1802), actin polymerization machinery (Arc40, Las17, Lsb3, Ysc84, Abp1) and chaperones (Hsp104, Ssa2). Selection for DHFR reconstitution with Sla1, in which the PLD was deleted (*Sla1 ΔPLD),* revealed that all interactions are lost with the exception of 2, Sla2 and Apb1 (Figure S3B-C). The loss of interactions is consistent with yeast two-hybrid studies of Sla1 in which the C-terminal repeats, within our PLD, are deleted resulting in loss of Sla1 protein-protein interactions (Tang, Xu et al. 2000). We observed that phase separation of Sla1 *in vitro* is equivalent after deletion of the PLD while phase separation of Ent1 in which the PLD was deleted (Ent1-ΔPLD*)* is completely prevented under the same conditions (Figure S3D). We thus conclude that *in vivo,* the PLD of Sla1 is essential for normal CME function and Sla1 protein-protein interactions (Figure 2 and S3B-C).

We next distinguished between the two opposing PLD-driven phase-separation *versus* obligate protein-protein interaction network hypotheses (Figure 3A). We did this by comparing results of phase separation and endocytosis for the substitution of PLD domains in either Ent1 or Sla1.

We thus engineered two types of chimeric proteins that contain either Sla1 PLD or sequence variants of Sup35 NM fused to N-terminal ENTH region (ENTH1) of yeast Epsin protein Ent1. We included sequence variants of Sup35 NM – a PLD of the classic prion protein Sup35 in which

either all asparagine (N) residues are substituted with glutamine (Q) or *vice versa* in the NM domain, yielding mutants Sup35 NM(Q) and Sup35 NM(N). We chose these sequences for two reasons. First, Sup35 is the archetypal prion protein used to determine sequence compositions of all PLDs in the yeast genome. Second, because the mutant Sup35 NM(Q) shares amino acid composition with Sla1 PLD and both undergo non-nucleation-limited self-assembly (Alberti, Halfmann et al. 2009, Khan, Kandola et al. 2018). We also engineered chimeric Epsin proteins from the yeast paralog Ent2 (for which the PLD is essential for phase separation but not for CME function) and human homologs EPN1/3 as controls (Figure 3C).

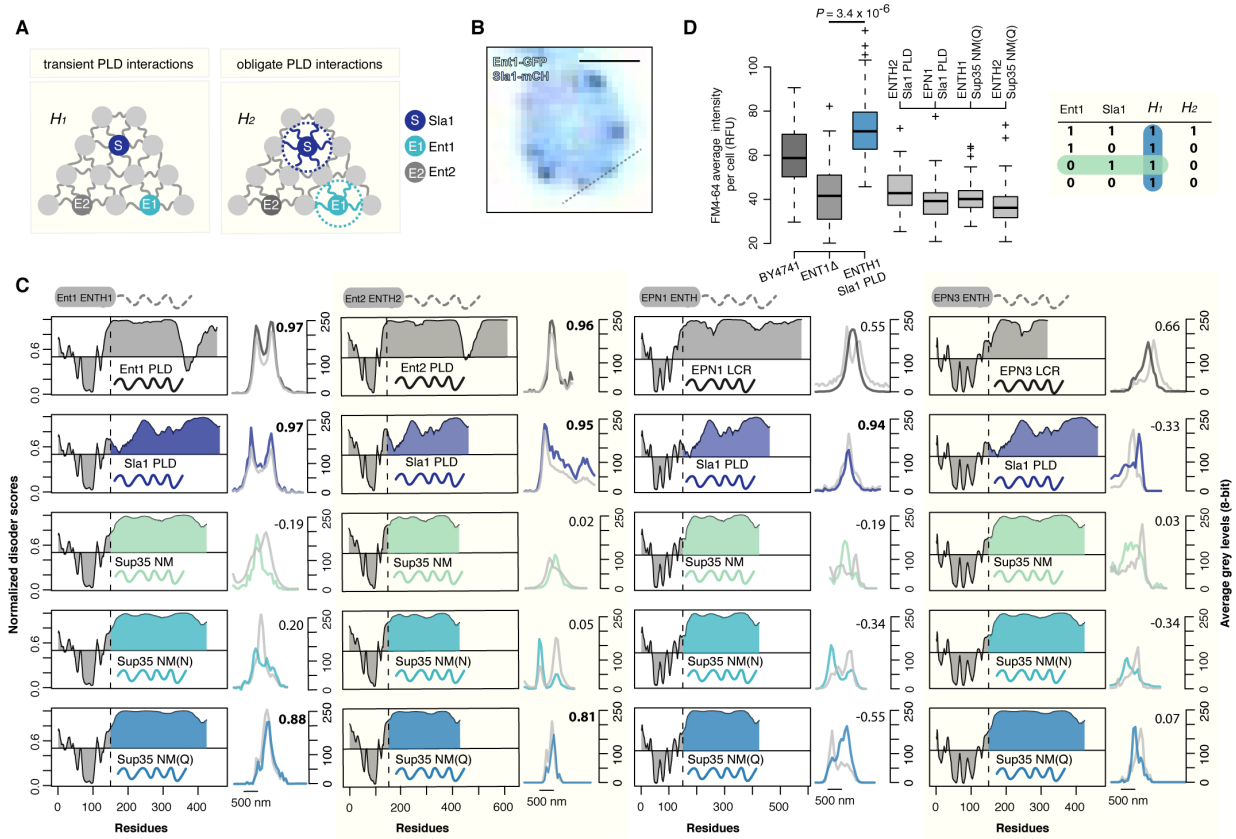

Figure 3 | PLDs are interchangeable and modulate assembly of chimeric proteins into phase-separated bodies (A) Illustration of the hypothesis *(H1)* that coat proteins condense together through transient PLD interactions, and the alternate hypothesis *(H2)* that coat proteins assemble into a complex through obligate protein-protein interactions. (B) Colocalization of Ent1-GFP signal within a Sla1-mCherry foci in yeast cells, line scan was performed as indicated. Scale bar 1 μM. (C) In the first column, the left panels show the PNDR-fit score (VLS2) for *wildtype* (grey) and chimeric proteins; chimeras include ENTH1 fused to either Sla1 PLD or Sup35 NM or Sup35 NM(N) or Sup35 NM(Q). Scores above 0.5 indicate the protein region is predicted to be disordered. Right panels show line scans to assess if *wildtype* or chimeric proteins colocalize with Sla1 foci (grey) in yeast cells. Example of a line scan is given in B. Pearson correlation values are given to confirm if the signals colocalize. The next columns show the same analysis for yeast ENTH2, human EPN1 ENTH and human EPN3 ENTH respectively. (D) Quantification (left panel; box center line, median; box limits, upper and lower quartiles; whiskers, 1.5x IQR; crosses, outliers) by fluorescence microscopy of FM4-64 dye uptake in cells for strains that overexpress fusions of

either Sla1 PLD or Sup35 NM(Qs) to the N-terminal region of yeast Ent1 (ENTH1) or Ent2 (ENTH2) proteins or human EPN1 (ENTH) proteins (n = 100 cells; two-sided t-test; see Methods). Presence of cognate PLD (1) or non-cognate PLD (0) fused to either Ent1 or Sla1 are the input variables in the truth table (right panel). Measures of colocalization and CME levels for ENTH1 Sla1 PLD (green) confirm the hypothesis *(H1)* (blue) that transient PLD interactions drive condensation of coat proteins. See also Figure S3.

We observed that ENTH1 and ENTH2 domains of Ent1 and Ent2 proteins, respectively fused to either Sla1 PLD or Sup35 NM(Q) localized into- and matured with endocytic condensates (as visualized with Sla1-mCherry) (Figure 3B-C). Absence of colocalization for the other chimeric Epsins suggests that a limited degree of sequence divergence is tolerated for ENTH domains fused to artificial or non-cognate PLDs to partition into endocytic condensates (Figure 3C). Note that Sla1 PLD did, while all Sup35 NM variants did not partition with endocytic condensates on their own (Figure S3E-F). We also observed that the human Epsin homologs EPN1/3 share conserved patterns of disorder with yeast Epsin proteins Ent1/2 (Figure 3C) and thus, we tested whether they would partition with endocytic condensates. We engineered chimeric proteins of EPN1/3 in which their low complexity domains (LCDs) were replaced with either Sla1 PLD or sequence variants of Sup35 NM. Although EPN1 and EPN3 *wildtype* and chimeric constructs all formed foci in yeast cells, only the chimeric EPN1 ENTH fused to the Sla1 PLD localized into- and matured with endocytic condensates (Figure 3C and Figure S3G-I).

We next tested whether the chimeric Epsins could function by measuring FM4-64 dye uptake in *ENT1*Δ cells (Figure 3D). Only Ent1 ENTH1 domain fused to Sla1 PLD colocalized with endocytic condensates and resulted in recovery of endocytic activity. In controls, we observed no function rescue by other Sla1 PLD fusions (Figure 3D). Thus, we propose that this result is the "exception that disproves the rule" that formation of an obligate protein-protein interaction network by Sla1-PLD is essential for endocytosis to occur. We propose that cognate PLDs mediate phase separation of coat proteins into endocytic condensates (Figure 3D). Additional evidence that goes against the idea that obligate protein-protein interactions underlie coat protein assembly includes the recent observations that coat proteins assemble without perfect stoichiometry of components, unlike the clathrin or Arp2/3 actin complexes (Holland and Johnson 2018). Further, there is no electron micrographic evidence for large protein structures, besides the clathrin mesh, to support the existence of a structured macromolecular complex made of coat proteins (Sochacki, Dickey et al. 2017). Even when actin bundles are present on cortical sites, the actin patches do not have a clear structure and are best described as an active viscoelastic gels (Carlsson and Bayly 2014).

We do not mean to imply that the protein-protein interaction network formed in endocytic condensates is unimportant; evidently it is involved in the regulation of endocytosis. For instance, all of the interactions of coat proteins with the proteins that nucleate actin polymerization are absolutely essential in actin-dependent endocytosis. Our results suggest that in actin-independent endocytosis, phase separation into endocytic condensates is essential for endocytosis and that the

316 formation of the endocytic protein-protein interaction network follows specific PLD-dependent
317 phase separation.
318
319 The observation that the Sup35 NM variants cannot fully complement the Sla1 PLD is consistent
320 with a recent study that uncovered a "molecular grammar" underlying protein liquid-liquid phase
321 separation in so-called FUS family proteins (Wang, Choi et al. 2018). The valency i.e., the numbers
322 of Tyr and Arg residues were shown to be the main determinants of the driving forces for phase
323 separation of FUS family proteins, likely through direct interaction with each other. The authors
324 refered to these residues as "*stickers"*. The types of residues that are interspersed between Tyr and
325 Arg appear to determine the material properties of condensates. The authors referred to these as
326 "*spacers*". Wang *et al*. suggest that the identities of stickers and spacers are likely to be governed
327 by the functions of condensates formed by the IDPs. Indeed, this specificity is manifest in our
328 results that compare the properties of Sup35 NM(Q) mutant to the PLD of Sla1. The amino acid
329 composition of Sup35 NM(Q) mutant is similar to that of Sla1 PLD. However, although this
330 sequence supports phase separation of the chimeria ENTH1::Sup35 NM(Q), it could not support
331 endocytosis (Figure 3C-D). Thus it appears that the PLD sequence of Sla1 and those of other PLD-
332 containing proteins are evolutionarily optimized to enable the formation of endocytic condensates
333 with properties that will give the resulting condensate the properties optimal to drive membrane
334 invaginations.
335
336 Taken together, the totality of our results support the hypothesis that the cortical bodies we study
337 here are phase-separated viscoelastic condensates. We next determined the material properties of
338 the endocytic condensates and tested our postulate that their interactions with the plasma
339 membrane generates the force that drives invagination of the membrane.
340
341 **Interfacial interactions of endocytic condensates cause deformation of the cytosol and**
342 **membrane**
343
344 We hypothesized that free energy released by endocytic condensate phase separation is converted
345 into mechanical work to deform the membrane and the cytosol. This mechanical work is
346 manifested as an inward pressure on the membrane created by expansion of the condensate with
347 the requirement that volume of the condensate is conserved. Phenomena in which geometric
348 organization of matter is driven by the balances of opposing forces have been described for a range
349 of length scales and examples of these include "fingering instabilities" (Kull 1991, Hester 2008,
350 Xi, Byrnes et al. 2017).
351
352 The mechanics of CME can be described by analogy to a soft viscoelastic and sticky balloon bound
353 to a soft elastic sheet (Movie S2). If you were to press your finger into the center of the sheet-
354 balloon interface to create an invagination, the surface area of the balloon would have to increase
355 to maintain a constant volume and density of the balloon. Equally, if you were to grasp the sticky

surface of the balloon with your hands and pull outwards equally over the surface, except at the elastic sheet-balloon interface, a tiny increase of the surface area would require a compensating adjustment of the shape so that the balloon would maintain a constant volume. Since force would be applied outwards everywhere except at the sheet balloon interface, it is there that an invagination of the membrane-balloon interface would compensate for the pressure generated by the outward force on the balloon surface.

In the case of CME, the grasping force is caused by interactions of molecules at the endocytic condensate-cytoplasm interface. Balance between this binding and elastic/surface deformation energies is achieved when the membrane invaginates. This idea is captured in a simple phenomenological model expressed as the sum of mechanical strain energy (ϕ term) and work (ψ term), respectively;

$$U = \phi \cdot \delta^{1+\varepsilon} - \psi \cdot \delta \; ; \tag{1}$$

Here, U is a mean-field energy, δ is the invagination depth of both the membrane and cytosol (which are coupled by virtue of conservation of volume of the condensate), and the exponent $\varepsilon > 0$ is determined by the deformation geometry (Methods). At equilibrium $\partial U/\partial\delta = 0$ and we expect invagination to balance the two contributions such that δ^* minimizes energy in (1) resulting in,

$$\delta^* = \left(\frac{\psi}{\phi\,(1+\varepsilon)} \right)^{\frac{1}{\varepsilon}} \; ; \tag{2}$$

Equation (2) shows that the invagination depth δ is determined by the ratio ψ/ϕ and the deformation geometry ε. To determine the numerical values of ϕ and ψ with mechanical contact theory, we must estimate the geometries of the condensate, the viscoelastic properties of the cytosol, the condensate and the membrane and from these values, determine the interfacial tensions among them (Methods).

Endocytic condensates are embedded in a viscoelastic cytosol

We used active rheology to measure the material properties of the cytosol in which endocytic condensates are embedded. We then calculated the condensate properties based on Hertz theory, which directly relates the material properties of one elastic material to that of an embedded elastic object, based on the deformation geometry, as described below. Specifically, we used optical tweezers to examine the frequency-dependent amplitude and phase responses of polystyrene beads embedded in cells (Figure 4A and Methods). Polystyrene beads of 200 nm diameter were integrated into cells by osmoporation (Figure S4A-B). Measurements of passive diffusion of the beads showed mean square displacements (MSD) close to that of random mechanical noise caused

by vibration of the microscope (Figure S4C). Furthermore, we established that the osmoporation procedure did not affect rheological properties of cells by measuring the MSD of expressed viral capsid microNS particles labeled with GFP in untreated or osmoporated cells and showing that their diffusion behaviors were identical (Figure S4D-F) (Munder, Midtvedt et al. 2016).

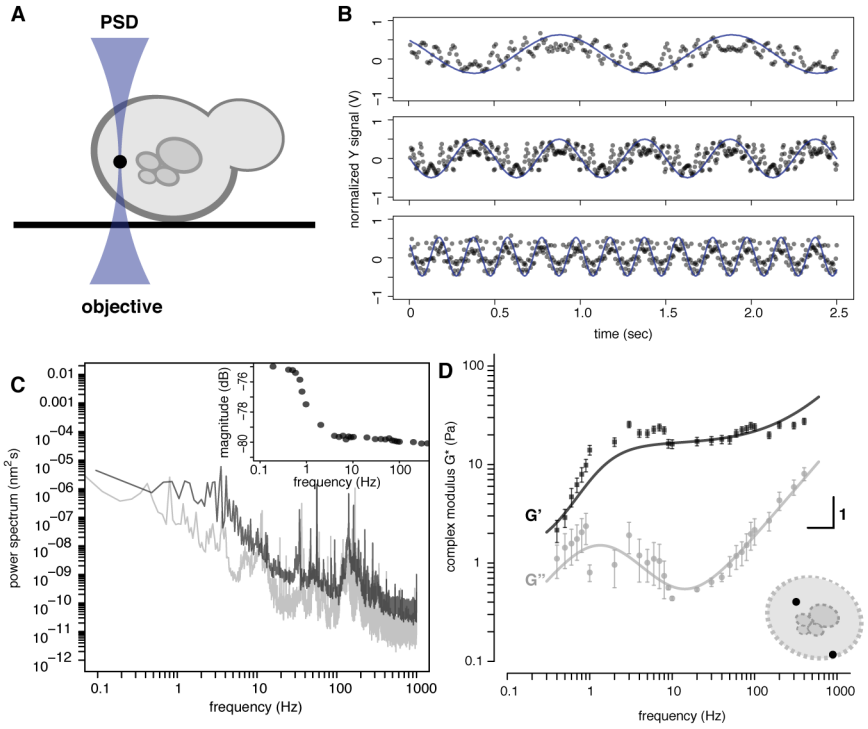

Figure 4 | Yeast cytosol is composed of a viscoelastic network of interacting proteins (A) We used optical tweezers (beam between the microscope objective and a position sensitive detector (PSD) coupled to an acousto-optic device (AOD) to oscillate polystyrene beads in cells. Two pulses of osmotic shock were used to osmoporate 200 nm polystyrene beads (black) into Lat A-treated haploid yeast *GPD1Δ* cells. (B) PSD output signal in volts (V) as a function of time for acquisitions made at 1Hz (top), 2 Hz (middle) and 5 Hz (bottom). A bead, located in the cell periphery, was oscillated with the AOD in the Y-axis of the specimen plane with fixed tweezer movement amplitude (normalized blue curve) at different frequencies. The recorded PSD raw traces (black points) were also normalized to a corresponding magnitude range (coherence cutoff of 0.9). (C) Power spectrum of the oscillated bead (black) with magnitude of response as a function of frequency (insert). (D) Decomposition of G* as a function of frequency into G′ (storage modulus; darker squares) and G″ (loss modulus; light shade circles) for beads distributed at both the cell periphery and interior (see schematic insert; mean ± sd; n = 17 cells) with an average trap stiffness k_{trap} (mean ± se; 8.0 x 10^{-5} ± 2.7 x 10^{-5} N m^{-1}) and photodiode sensitivity factor β (mean ± se; 10.7 x 10^{-3} ± 2.3 x 10^{-3} nm V^{-1}). Data was fitted to a model of an entangled and crosslinked network of flexible polymers (Methods; Eq. 2.9-2.10). See also Figure S4.

For active rheology experiments, we used an acousto-optic device to oscillate the position of the optical trap in the specimen plane at frequencies over four orders of magnitude and measured the displacement of trapped beads from the trap center using back focal plane interferometry (Figure 4B). We thus measured the viscoelastic properties of the cytosol surrounding the beads by

421 measuring the phase and amplitude of displacements of beads in response to the oscillations of the
422 optical tweezers. Then, by calculating the power spectrum of unforced fluctuations of the bead,
423 we obtained storage (G′) and loss (G″) moduli as a function of frequency (Figure 4C-D, S4G-H
424 and Methods) (Hendricks and Goldman 2017).
425
426 Cells and underlying structures show different mechanical properties depending on the rates at
427 which forces are applied to them (Hendricks, Holzbaur et al. 2012, Guo, Ehrlicher et al. 2013,
428 Guo, Ehrlicher et al. 2014). If a force is applied at a low velocity, the cell behaves like a viscous
429 fluid, flowing and taking on whatever shape it is forced into. When a force is applied at higher
430 velocity the material behaves like an elastic object, bouncing back to its original shape. As we
431 discuss below, these behaviors reflect the manner and strengths with which the molecules of the
432 material interact with each other and their environment.
433
434 The material properties of the yeast cytoplasm and its interactions with the endocytic condensate
435 derive from the complex modulus *versus* frequency plot as follows (Figure 4D). When deformed
436 by the condensate growth (at a velocity of growth = 2360 ± 120 nm s^{-1}; corresponding to a stress
437 at ~30 ± 2 Hz) the cytosol is elastic; membrane invagination occurs at a rate (a velocity of 7.4 ±
438 2.5 nm s^{-1}; corresponding to 0.1 ± 0.04 Hz) at which the cytoplasm is viscoelastic and very
439 compliant (Figure 4D and S4I-J). The G′ and G″ we measured here in yeast are similar to those of
440 the cytoplasm of adherent mammalian cells (Hendricks, Holzbaur et al. 2012, Guo, Ehrlicher et al.
441 2013, Guo, Ehrlicher et al. 2014).
442
443 The material properties of the endocytic condensate were calculated using its geometric
444 dimensions (Figure 1B) and the material properties of the cytosol (Figure 4). As noted above,
445 classic Hertz theory relates contact geometries of elastic materials to their respective mechanical
446 properties. Therefore, we used the geometry of the endocytic condensates determined in our super-
447 resolution fluorescence imaging experiments and the moduli of the cytosol in which they are
448 embedded to estimate the endocytic condensate elastic modulus which was 59 Pa (Figure 1B, 4D,
449 and Methods; Eq. 3.7-3.10) (Hertz 1882). These results are consistent with protein condensates
450 that form elastic materials (Reichheld, Muiznieks et al. 2017) and suggests that endocytic
451 condensates have similar material properties as the surrounding cytosol, which has an elastic
452 modulus of 45 Pa at 1 Hz (Methods).
453
454 **PLD-containing coat proteins form a dense network of interacting molecules**
455
456 We estimated the average mesh size and permeability of the endocytic condensates by probing
457 them with fluorophore-conjugated dextran molecules of 2.4, 5.8, and 10.4 nm in diameter. We
458 measured FRAP and colocalization of these dextran molecules with either Sla1-mCherry or Syp1-
459 mCherry puncta (Figure 5 and S5). Although the density of 5.8 nm dextran-FITC is lower in Sla1
460 puncta than in the surrounding cytosol, the mobility of the 5.8 nm probe is equal in both regions

461 (Figure 5A and S5B-D). We observed that both 2.4 nm and 5.8 nm dextran-FITC recovered equally
462 well in the condensate and cytosolic zones (Figure 5A and S5F). In contrast, few 10.4 nm dextran-
463 FITC molecules permeate the PLD-rich protein network in the condensate, whereas they are
464 mobile in the neighboring cytosol (Figure 4B). When endocytic condensates are disrupted by
465 addition of 1,6-hexanediol, we observe equivalent mobility of 10.4 nm dextran-FITC between
466 cortical sites, labelled with the protein Syp1-mCherry, which is membrane-bound at cortical
467 patches in an HD-resistant manner, and neighboring cytosol (Figure 5 and S5E). These results are
468 consistent with an exclusion zone for ribosomes as discussed above and with exclusion of dextrans
469 by known protein-RNA phase separated condensates called P granules (Updike, Hachey et al.
470 2011, Wei, Elbaum-Garfinkle et al. 2017).
471

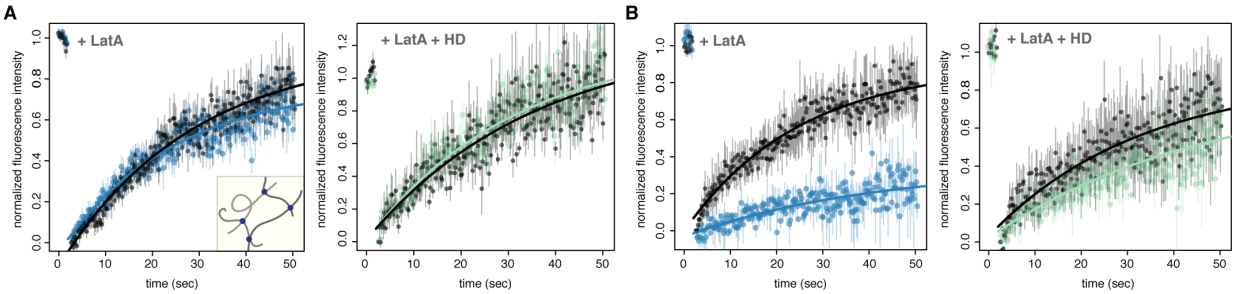

472
473
474 **Figure 5 | Porous meshwork structure of endocytic condensates is less permeable than cytosol** (A)
475 Fluorescence recovery after photobleaching (FRAP) of dextran-FITC probes within endocytic condensates
476 or neighbouring cytosol regions of interest. FRAP of the bleached 5.8 nm dextran-FITC within either a
477 Sla1-mCherry (left panel; Lat A treated cells; blue) or a Syp1-mCherry (right panel; Lat A and 5% HD
478 treated cells; green) puncta and neighbouring cytosol regions (black) without Sla1 or Syp1 signals
479 respectively. Insert is an illustration of a porous latticework composed of amorphous protein chains (grey
480 filaments) with binding sites (dots) through which they are non-covalently associated. (B) Same experiment
481 with 10.4 nm dextran-FITC that scarcely permeate the Sla1 puncta (left panel; Lat A treated cells; blue) but
482 are mobile when condensates are dissolved by HD (right panel; Lat A and 5% HD treated cells; green).
483 Data points (mean ± SEM; n = 10 cells) were fitted to a single term recovery function (Methods). See also
484 Figure S4.
485

486 **Interactions of endocytic condensates with cytosol and membrane provide the required**
487 **energy to drive membrane invagination**
488

489 The deformation of the membrane in response to contact with a soft object depends on the
490 geometries and mechanical properties of the object and the vessel it is in (in our case the cytosol
491 of a cell) and the membrane (Figure 6A). Evidence from electron and super-resolution
492 fluorescence microscopy indicates that the favored geometry of the membrane is flat with an
493 invagination centered in the middle of the condensate (Figure 6A, lower). Such geometries are
494 explained by a local radial stress-gradient generated by the condensate adhesion to both the
495 membrane and cytosol or by local binding of adaptor proteins and distinct lipid compositions.

Simply stated, as the condensate grows, the interactions to the cytosol draws it inward and the membrane follows, mediated by its own interactions to the condensate and the requirement that the volume of the condensate be conserved.

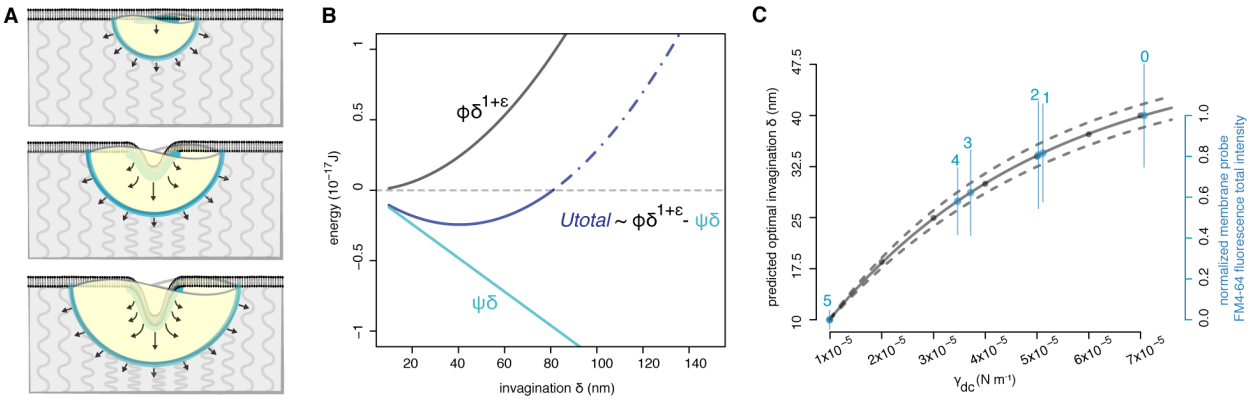

Figure 6. Endocytic condensates do mechanical work to deform the membrane and cytosol (A) Illustration of a endocytic condensate (yellow) that binds to (wets) a bilayer membrane (black) and drives membrane invagination (top to bottom). Resultant membrane deformations reflect how forces balance under a Young-Dupré adhesion gradient (blue lines and arrows). Resistance to deformation is represented by grey curved lines. (B) Equation (1) (insert) was used to calculate the energy penalties (ϕ) and contributions (ψ) at the cytosol and membrane interfaces with the endocytic condensate. Total energy of the system (dark blue), energy penalties (black) and energy contributions (light blue) are presented as a function of membrane invagination (δ). The energy of membrane invagination is favourable for δ between about 15-80 nm (solid blue line) and unfavorable above 80 nm (dashed blue line). Quantities used to calculate energies are detailed in Figure S5, Table S3 and S4. (C) Our model predicts that vesicle size is proportional to the strength of condensate intermolecular protein-protein interactions that are proportional to γ_{dc}, the condensate-to-cytosol interfacial tension. Predicted membrane invagination δ as a function of γ_{dc} (left axis and black points). Data points were fitted to an exponential decay function (full line) with 95% confidence interval (dashed lines). Titration of 1,6-hexanediol was used to reduce intermolecular cohesion and therefore γ_{dc} resulting in reduced vesicle size as measured by uptake of the lipophilic membrane probe FM4-64 into *GPD1*Δ Sla1-YFP cells treated with Lat A (Right axis, red) *versus* % HD (blue numbers, n= 25, mean ± sd) expressed as a function of the condensate-cytosol interfacial tension γ_{dc} (Methods). See also Figure S5.

We quantified the work performed by the condensate to invaginate the membrane using the storage and loss moduli obtained from the micro-rheology experiments, geometric data obtained from super-resolution imaging, and other data available from the literature. We used these values to solve the explicit form of the ϕ and ψ terms (mechanical strain and work, respectively) in Equation (1) as functions of membrane and cytosol invagination δ (Methods; Eq. 4.25-4.26). Using the Young-Laplace equation, we first estimated an interfacial tension for the condensate-cytosol interface to be approximately γ_{dc} of 7×10^{-5} N•m^{-1}. This estimate is based on the pressure difference across the cytosolic interface and the condensate mean curvature (Methods; Eq. 4.6). Our estimate for the interfacial tension falls within the range of values that have been reported for other protein

530 condensates, including nucleoli and P granules (Methods; Eq. 4.9) (Brangwynne, Mitchison et al.
531 2011, Elbaum-Garfinkle, Kim et al. 2015).
532
533 Given our estimates of γ_{dc}, we also determined the work of adhesion released when the condensate
534 surfaces are created, as described by the Young-Dupré equation (Figure 6 and Methods; Eq. 4.11).
535 We calculated an adhesion energy (ψ) of 4.9×10^{-18} J from interactions between the endocytic
536 condensate and both the membrane and cytosol (Figure 6B, S6 and Methods; Eq. 4.26). Our results
537 suggest that the most significant contribution of the mechanical energy comes from the
538 condensate-cytosol interface, where the adhesion energy of 2.9×10^{-18} J is enough to overcome an
539 energy penalty of 2.4×10^{-18} J to deform the membrane and the cytosol. This energy cost includes
540 the elastic, viscous, and interfacial stress penalties (Figure 6B, S6 and Table S4). We also
541 calculated an average adhesion energy of 1.3 $kJ \bullet mol^{-1}$ at the condensate-cytosol interface
542 (Methods), which is consistent with the free energies expected of non-covalent interactions
543 (Mahadevi and Sastry 2016).
544
545 Our model provides a physical framework to explain how endocytic condensates exert force to
546 induce invagination of membranes in actin-independent CME in our mutant yeast cells. The
547 interface between condensates, formed by phase separation of disordered proteins into cortical
548 bodies, and the cytosol or membrane deforms the surrounding materials through adhesive
549 interactions. Invagination occurs when ψ dominates ϕ in Equation (1) and is favored within the
550 observed δ interval of 40 nm to 80 nm (Figure S6). Notably, this predicted δ interval is within the
551 range of plasma membrane invagination of 70 nm or more, at which point membrane constriction
552 and vesicle scission mechanisms are activated to complete CME (Idrissi, Blasco et al. 2012).
553
554 **Condensate cohesion and interfacial tension determines the potential energy**
555
556 We propose that endocytic condensates store and dissipate mechanical energy in the form of
557 interfacial tension, whereby the composition of the condensates determine their interfacial
558 interactions, and provides the energy for adhesion and invagination of membranes. Accordingly,
559 the underlying energy stored within the condensates and the balance of interactions amongst
560 condensate components and solvent governs the interface. The effective potential energy ψ of
561 condensates, which is equivalent to the total work of adhesion, should be dictated by the density
562 and strengths of physical interactions amongst proteins within the condensate (the condensate
563 cohesion and interfacial tensions). We tested this hypothesis by using 1,6-hexanediol (HD) to
564 weaken the favorable free energies of the protein-protein interactions within condensates. These
565 interactions drive the phase separation of endocytic condensates, and HD titration would
566 correspond to a decrease of the condensate surface tension (γ_{dc} or ψ). Our model predicts that
567 invagination depth should vary continuously with ψ - Equation (2). We titrated HD below the
568 effective concentration that prevents protein phase separation and quantified individual membrane
569 excision events by measuring the uptake of the lipophilic membrane probe FM4-64 into cells by

570 fluorescence microscopy (Figure 2A and Methods). In Lat A treated *GPD1Δ* cells, our
571 measurement reports the amount of labeled membrane taken up into cells under the action of
572 endocytic condensates alone. By increasing subcritical HD concentration (corresponding to a
573 decrease in ψ), the average fluorescence-labeled membrane per vesicle (a proxy for invagination
574 δ) was continuously reduced over one order of magnitude in the value of γ_{dc} (Figure 6C and
575 Methods; Eq. 2.8). This observation fits with the reduced membrane invagination that we predicted
576 at the outset (*i.e.*, that δ scales with the ψ/ϕ ratio) when the condensate cohesion (γ_{dc} or ψ) is also
577 reduced (Figure 6C and Methods; Eq. 4.2).
578
579 **Discussion**
580 **Existing models of actin-independent CME are implicit to our viscoelastic protein**
581 **condensate model**
582
583 In the context of actin-independent CME in *S. cerevisiae*, we estimated that approximately 9.7 ×
584 10^{-18} J of energy is required to produce an 80 nm deep membrane invagination. We have also
585 estimated that protein condensate formation generates 4.9 × 10^{-18} J to reach the energy minima
586 (Figure 6C and Table S4). This suggests that other curvature-generating mechanisms must provide
587 the energy balance to maintain or increase the profundity of the energy minimum in our model.
588 Several proposed mechanisms could provide significant sources of energy to account for this
589 deficit; such mechanisms may also depend on formation of the endocytic condensates. These
590 include *(1)*, membrane curvature-inducing proteins and protein complexes, including convex-
591 shaped BAR (for Bin, Amphiphysin and Rvs) domain-containing proteins (Youn, Friesen et al.
592 2010, Yu and Schulten), *(2)*, insertion of amphipathic protein helix into membrane (Ford, Mills et
593 al. 2002, Boucrot, Pick et al. 2012)*(3)*, local relief of turgor pressure (Scher-Zagier and Carlsson
594 2016), *(4)*, proteins that modulate lipid composition (Graham and Kozlov 2010, Anitei, Stange et
595 al. 2017) or *(5)*, steric exclusion or crowding of proteins at cortical sites (Snead, Hayden et al.
596 2017). A counterargument to the latter point *(5)* is that calculations of the entropic gain and
597 pressure produced in the crowded protein layer, obtained with the Carnahan-Starling equation
598 which assumes that proteins are non-attracting (non-interacting) disks (Derganc and Copic 2016),
599 are not compatible with the interaction energies that we estimate to account for cohesion among
600 the condensate-forming proteins or adhesion at membrane and cytosol interfaces with the
601 condensate.
602
603 It is possible that most of these mechanisms have an additive effect *in vivo* and are integrated with
604 the condensate-based mechanism we introduce here to drive actin-independent CME. Binding of
605 Epsins (Ent1 and Ent2 proteins in yeast), in particular, has been proposed to facilitate deformation
606 of membranes by insertion of an amphipathic helix into the outer leaflet of the bilayer, which
607 pushes the head groups apart (Ford, Mills et al. 2002, Boucrot, Pick et al. 2012, Skruzny, Desfosses
608 et al. 2015). ENTH-containing Epsin proteins are also reported to reduce membrane tension of
609 artificial giant vesicles, thus facilitating deformation and curvature of the membrane (Gleisner,

Kroppen et al. 2016). By reducing the effective resistance of membrane elasticity, Epsin-membrane interactions could shift right and increase the profundity of the energy minimum in our model. At the same time, for these mechanisms to work, the proteins must be concentrated at endocytic sites, a function served by their phase separation with the condensate.

Implications of endocytic condensates to other emergent phenomena

Our results provide a framework for answering many questions regarding CME and other membrane budding processes. For example, given our observations, how is CME coupled to signaling pathways that regulate vesicle formation? The PLD-containing CME proteins we investigated are enriched for multiple phosphorylation sites, which undergo changes in response to activation of a CME-regulating signaling pathway (Kanshin, Bergeron-Sandoval et al. 2015). Since the amount and distribution of charge in disordered regions of proteins regulate their interactions and conformations (Das and Pappu 2013), such post-translational modifications may be important to regulating phase separation and material properties of CME condensates (Miao, Tipakornsaowapak et al. 2018).

Our fluorescence microscopy and electron micrographic evidence from the literature suggests that the endocytic condensate remains associated temporarily with mature vesicles (Kukulski, Schorb et al. 2012). Does the condensate play any role in trafficking and fusing with, for instance, plasma membrane (protein recycling) or lysosome (protein degradation)? CME also underlies several fundamental mechanisms of vesicle trafficking and attendant membrane and vesicle protein cargo transport, including late secretory pathways and neuronal synaptic vesicle recycling in which both scission of budding vesicles and their re-fusion to other membranes occurs.

Yeast and human proteins implicated in clathrin-mediated vesicle trafficking are enriched for long disordered protein domains (47 % of human and 23% of yeast proteins have long consecutive disordered regions of up to or greater than 30 residues), whereas those involved in two other vesicle trafficking systems are not (COPI: 8/5%; COPII: 8/5%) (Pietrosemoli, Pancsa et al. 2013). These observations argue for investigating the generality and conservation of protein condensate adhesion-driven membrane invagination as an underlying source of energy in clathrin-mediated vesicle trafficking in the absence of actin polymerization.

Recent evidence suggests that neurodegenerative pathologies, such as Amyotrophic lateral sclerosis, Huntington's and Alzheimer's, may result from both aberrant liquid-liquid phase separation of proteins and disruption of endocytosis (Bhattacharyya, Banerjee et al. 2008, Wu and Yao 2009, G. Liu, A.N. Coyne et al. 2017). In future work, it will be interesting to observe whether adherent liquid-liquid phase separation of proteins in endocytic condensates contribute to these pathologies.

Phase separation of proteins in an elastic network, such as yeast cytosol, is predicted to restrain the size of condensates because condensates have a limited mechanical potential to deform the cytosol in order to grow beyond the cytosol mesh size (Style, Sai et al. 2018). Our results suggest that, beyond deformation of cellular structures, the material properties of the cytosol and the interactions amongst proteins within the condensate can also dictate the dimensions of biopolymer condensates found in cells.

Finally, it is possible that other liquid-liquid phase separated protein and protein nucleic acid condensates influence cellular sub-structural dynamics and thus contribute to shaping cell, tissue, and organism morphology (Bergeron-Sandoval, Safaee et al. 2016, Bauerlein, Saha et al. 2017, Bergeron-Sandoval and Michnick 2018, Style, Sai et al. 2018). More broadly, interfacial contact potentials between different biological materials may represent a vastly underestimated source of complex pattern formation in biology, such as has been observed in embryonic tissue layers (Foty, Pfleger et al. 1996), in a model of growing brain convolutions (Tallinen, Chung et al. 2016), in protein stabilization (Gupta, Donlan et al. 2017) and in the ability of clathrin-coated structures to wrap around and pinch collagen fibers (Elkhatib, Bresteau et al. 2017).

Acknowledgements

The authors acknowledge support from CIHR grants MOP-GMX-152556 (SWM), the US National Institutes of Health grant R01NS056114 (RVP), the Fonds Québécois de la Recherche sur la Nature et les Technologies (SWM an PF) and the Human Frontier Science Program RGP0034/2017 (SWM and RVP). CEC was supported by the National Institute of General Medical Sciences of the National Institutes of Health (NIH) under award T32GM008268. Research in the Keller Lab is supported by National Science Foundation award MCB-1402059 to SLK. We thank Cliff Brangwynne, David Drubin, Tom Pollard and Julien Berro for thoughtful discussion and advice on the manuscript; Jackie Vogel for strains; Susan Liebman and Randal Halfmann for plasmids; Jacqueline Kowarzyk and Philippe Garneau for technical assistance and Rosa Kaviani for help with FRAP experiments.

Author Contributions

LPBS and SWM designed the research with the assistance of RVP; LPBS performed biological research; LPBS, AJE, RVP and SWM analysed the biological data; CC, CEC and SLK performed and analysed the vesicle leakage experiments; LPBS and HKH performed micro rheology experiments; LPBS, HKH, AJE and AGH analysed micro rheology data; LPBS, HKH and PF developed physical model; LPBS and SWM wrote the first version, all authors corrected the paper.

Supplementary Materials

Materials and Methods

Figures S1-S6

Tables S1-S4

Movies S1-S2

References

1. Aghamohammadzadeh, S. and K. R. Ayscough (2009). "Differential requirements for actin during yeast and mammalian endocytosis." Nat Cell Biol **11**(8): 1039-1042.
2. Alberti, S., R. Halfmann, O. King, A. Kapila and S. Lindquist (2009). "A systematic survey identifies prions and illuminates sequence features of prionogenic proteins." Cell **137**(1): 146-158.
3. Alberti, S., S. Saha, J. B. Woodruff, T. M. Franzmann, J. Wang and A. A. Hyman (2018). "A User's Guide for Phase Separation Assays with Purified Proteins." J Mol Biol.
4. Anitei, M., C. Stange, C. Czupalla, C. Niehage, K. Schuhmann, P. Sala, A. Czogalla, T. Pursche, U. Coskun, A. Shevchenko and B. Hoflack (2017). "Spatiotemporal Control of Lipid Conversion, Actin-Based Mechanical Forces, and Curvature Sensors during Clathrin/AP-1-Coated Vesicle Biogenesis." Cell Rep **20**(9): 2087-2099.
5. Basu, R., E. L. Munteanu and F. Chang (2014). "Role of turgor pressure in endocytosis in fission yeast." Mol Biol Cell **25**(5): 679-687.
6. Bauerlein, F. J. B., I. Saha, A. Mishra, M. Kalemanov, A. Martinez-Sanchez, R. Klein, I. Dudanova, M. S. Hipp, F. U. Hartl, W. Baumeister and R. Fernandez-Busnadiego (2017). "In Situ Architecture and Cellular Interactions of PolyQ Inclusions." Cell **171**(1): 179-187 e110.
7. Bergeron-Sandoval, L. P. and S. W. Michnick (2018). "Mechanics, Structure and Function of Biopolymer Condensates." J Mol Biol.
8. Bergeron-Sandoval, L. P., N. Safaee and S. W. Michnick (2016). "Mechanisms and Consequences of Macromolecular Phase Separation." Cell **165**(5): 1067-1079.
9. Bhattacharyya, N. P., M. Banerjee and P. Majumder (2008). "Huntington's disease: roles of huntingtin-interacting protein 1 (HIP-1) and its molecular partner HIPPI in the regulation of apoptosis and transcription." FEBS J **275**(17): 4271-4279.
10. Boeke, D., S. Trautmann, M. Meurer, M. Wachsmuth, C. Godlee, M. Knop and M. Kaksonen (2014). "Quantification of cytosolic interactions identifies Ede1 oligomers as key organizers of endocytosis." Mol Syst Biol **10**: 756.
11. Boucrot, E., A. Pick, G. Camdere, N. Liska, E. Evergren, H. T. McMahon and M. M. Kozlov (2012). "Membrane fission is promoted by insertion of amphipathic helices and is restricted by crescent BAR domains." Cell **149**(1): 124-136.
12. Brangwynne, C. P., C. R. Eckmann, D. S. Courson, A. Rybarska, C. Hoege, J. Gharakhani, F. Julicher and A. A. Hyman (2009). "Germline P granules are liquid droplets that localize by controlled dissolution/condensation." Science **324**(5935): 1729-1732.
13. Brangwynne, C. P., T. J. Mitchison and A. A. Hyman (2011). "Active liquid-like behavior of nucleoli determines their size and shape in Xenopus laevis oocytes." Proc Natl Acad Sci U S A **108**(11): 4334-4339.
14. Carlsson, A. E. and P. V. Bayly (2014). "Force generation by endocytic actin patches in budding yeast." Biophys J **106**(8): 1596-1606.
15. Conner, S. D. and S. L. Schmid (2003). "Regulated portals of entry into the cell." Nature **422**(6927): 37-44.
16. Darwin, C. (1859). On the origin of species by means of natural selection, or, The preservation of favoured races in the struggle for life. London, J. Murray.
17. Das, R. K. and R. V. Pappu (2013). "Conformations of intrinsically disordered proteins are influenced by linear sequence distributions of oppositely charged residues." Proc Natl Acad Sci U S A **110**(33): 13392-13397.
18. Derganc, J. and A. Copic (2016). "Membrane bending by protein crowding is affected by protein lateral confinement." Biochim Biophys Acta **1858**(6): 1152-1159.
19. Elbaum-Garfinkle, S., Y. Kim, K. Szczepaniak, C. C. Chen, C. R. Eckmann, S. Myong and C. P. Brangwynne (2015). "The disordered P granule protein LAF-1 drives phase separation into droplets with tunable viscosity and dynamics." Proc Natl Acad Sci U S A **112**(23): 7189-7194.
20. Elkhatib, N., E. Bresteau, F. Baschieri, A. L. Rioja, G. van Niel, S. Vassilopoulos and G. Montagnac (2017). "Tubular clathrin/AP-2 lattices pinch collagen fibers to support 3D cell migration." Science **356**(6343).
21. Feric, M., N. Vaidya, T. S. Harmon, D. M. Mitrea, L. Zhu, T. M. Richardson, R. W. Kriwacki, R. V. Pappu and C. P. Brangwynne (2016). "Coexisting Liquid Phases Underlie Nucleolar Subcompartments." Cell **165**(7): 1686-1697.
22. Ford, M. G., I. G. Mills, B. J. Peter, Y. Vallis, G. J. Praefcke, P. R. Evans and H. T. McMahon (2002). "Curvature of clathrin-coated pits driven by epsin." Nature **419**(6905): 361-366.
23. Foty, R. A., C. M. Pfleger, G. Forgacs and M. S. Steinberg (1996). "Surface tensions of embryonic tissues predict their mutual envelopment behavior." Development **122**(5): 1611-1620.
24. G. Liu, A.N. Coyne, F. Pei, S. Vaughan, M. Chaung, D. C. Zarnescu and J. R. Buchan (2017). "Endocytosis

regulates TDP-43 toxicity and turnover." Nature communications **8**(2092).
25. Gleisner, M., B. Kroppen, C. Fricke, N. Teske, T. T. Kliesch, A. Janshoff, M. Meinecke and C. Steinem (2016). "Epsin N-terminal Homology Domain (ENTH) Activity as a Function of Membrane Tension." J Biol Chem **291**(38): 19953-19961.
26. Graham, T. R. and M. M. Kozlov (2010). "Interplay of proteins and lipids in generating membrane curvature." Curr Opin Cell Biol **22**(4): 430-436.
27. Guo, M., A. J. Ehrlicher, M. H. Jensen, M. Renz, J. R. Moore, R. D. Goldman, J. Lippincott-Schwartz, F. C. Mackintosh and D. A. Weitz (2014). "Probing the stochastic, motor-driven properties of the cytoplasm using force spectrum microscopy." Cell **158**(4): 822-832.
28. Guo, M., A. J. Ehrlicher, S. Mahammad, H. Fabich, M. H. Jensen, J. R. Moore, J. J. Fredberg, R. D. Goldman and D. A. Weitz (2013). "The role of vimentin intermediate filaments in cortical and cytoplasmic mechanics." Biophys J **105**(7): 1562-1568.
29. Gupta, K., J. A. Donlan, J. T. Hopper, P. Uzdavinys, M. Landreh, W. B. Struwe, D. Drew, A. J. Baldwin, P. J. Stansfeld and C. V. Robinson (2017). "The role of interfacial lipids in stabilizing membrane protein oligomers." Nature **541**(7637): 421-424.
30. Hendricks, A. G. and Y. E. Goldman (2017). "Measuring Molecular Forces Using Calibrated Optical Tweezers in Living Cells." Methods Mol Biol **1486**: 537-552.
31. Hendricks, A. G., E. L. Holzbaur and Y. E. Goldman (2012). "Force measurements on cargoes in living cells reveal collective dynamics of microtubule motors." Proc Natl Acad Sci U S A **109**(45): 18447-18452.
32. Hertz, H. R. (1882). Ueber die Beruehrung elastischer Koerper (On Contact Between Elastic Bodies). Leipzig, Germany, 1895.
33. Hester, J. J. (2008). "The Crab Nebula: An astrophysical chimera." Annual Review of Astronomy and Astrophysics **46**: 127-155.
34. Holland, D. O. and M. E. Johnson (2018). "Stoichiometric balance of protein copy numbers is measurable and functionally significant in a protein-protein interaction network for yeast endocytosis." PLoS Comput Biol **14**(3): e1006022.
35. Idrissi, F. Z., A. Blasco, A. Espinal and M. I. Geli (2012). "Ultrastructural dynamics of proteins involved in endocytic budding." Proc Natl Acad Sci U S A **109**(39): E2587-2594.
36. Kanshin, E., L. P. Bergeron-Sandoval, S. S. Isik, P. Thibault and S. W. Michnick (2015). "A cell-signaling network temporally resolves specific versus promiscuous phosphorylation." Cell Rep **10**(7): 1202-1214.
37. Khan, T., T. S. Kandola, J. Wu, S. Venkatesan, E. Ketter, J. J. Lange, A. Rodriguez Gama, A. Box, J. R. Unruh, M. Cook and R. Halfmann (2018). "Quantifying Nucleation In Vivo Reveals the Physical Basis of Prion-like Phase Behavior." Mol Cell **71**(1): 155-168 e157.
38. Khurana, R., C. Coleman, C. Ionescu-Zanetti, S. A. Carter, V. Krishna, R. K. Grover, R. Roy and S. Singh (2005). "Mechanism of thioflavin T binding to amyloid fibrils." J Struct Biol **151**(3): 229-238.
39. Kroschwald, S., S. Maharana, D. Mateju, L. Malinovska, E. Nuske, I. Poser, D. Richter and S. Alberti (2015). "Promiscuous interactions and protein disaggregases determine the material state of stress-inducible RNP granules." Elife **4**: e06807.
40. Kukulski, W., M. Schorb, M. Kaksonen and J. A. Briggs (2012). "Plasma membrane reshaping during endocytosis is revealed by time-resolved electron tomography." Cell **150**(3): 508-520.
41. Kull, H. J. (1991). "Theory of the Rayleigh-Taylor Instability." Physics Reports-Review Section of Physics Letters **206**(5): 197-325.
42. Li, D., L. Shao, B. C. Chen, X. Zhang, M. Zhang and B. Moses (2015). "Extended-resolution structured illumination imaging of endocytic and cytoskeletal dynamics." Science (New York, NY).
43. Li, X. H., P. L. Chavali, R. Pancsa, S. Chavali and M. M. Babu (2018). "Function and Regulation of Phase-Separated Biological Condensates." Biochemistry.
44. Li, Y., R. Lipowsky and R. Dimova (2011). "Membrane nanotubes induced by aqueous phase separation and stabilized by spontaneous curvature." Proc Natl Acad Sci U S A **108**(12): 4731-4736.
45. Lin, Y., D. S. W. Protter, M. K. Rosen and R. Parker (2015). "Formation and Maturation of Phase-Separated Liquid Droplets by RNA-Binding Proteins." Molecular Cell **60**(2): 208-219.
46. Mahadevi, A. S. and G. N. Sastry (2016). "Cooperativity in Noncovalent Interactions." Chem Rev **116**(5): 2775-2825.
47. Malinovska, L., S. Kroschwald and S. Alberti (2013). "Protein disorder, prion propensities, and self-organizing macromolecular collectives." Biochim Biophys Acta **1834**(5): 918-931.
48. Miao, Y., T. Tipakornsaowapak, L. Zheng, Y. Mu and E. Lewellyn (2018). "Phospho-regulation of intrinsically disordered proteins for actin assembly and endocytosis." FEBS J.

49. Molliex, A., J. Temirov, J. Lee, M. Coughlin, A. P. Kanagaraj, H. J. Kim, T. Mittag and J. P. Taylor (2015). "Phase separation by low complexity domains promotes stress granule assembly and drives pathological fibrillization." Cell **163**(1): 123-133.
50. Mukherjee, D., B. G. Coon, D. F. Edwards, 3rd, C. B. Hanna, S. A. Longhi, J. M. McCaffery, B. Wendland, L. A. Retegui, E. Bi and R. C. Aguilar (2009). "The yeast endocytic protein Epsin 2 functions in a cell-division signaling pathway." J Cell Sci **122**(Pt 14): 2453-2463.
51. Mund, M., J. A. van der Beek, J. Deschamps, S. Dmitrieff, J. L. Monster, A. Picco, F. Nedelec, M. Kaksonen and J. Ries (2017). "Systematic analysis of the molecular architecture of endocytosis reveals a nanoscale actin nucleation template that drives efficient vesicle formation." bioRxiv.
52. Munder, M. C., D. Midtvedt, T. Franzmann, E. Nuske, O. Otto, M. Herbig, E. Ulbricht, P. Muller, A. Taubenberger, S. Maharana, L. Malinovska, D. Richter, J. Guck, V. Zaburdaev and S. Alberti (2016). "A pH-driven transition of the cytoplasm from a fluid- to a solid-like state promotes entry into dormancy." Elife **5**.
53. Pappu, R. V., X. Wang, A. Vitalis and S. L. Crick (2008). "A polymer physics perspective on driving forces and mechanisms for protein aggregation." Arch Biochem Biophys **469**(1): 132-141.
54. Peskett, T. R., F. Rau, J. O'Driscoll, R. Patani, A. R. Lowe and H. R. Saibil (2018). "A Liquid to Solid Phase Transition Underlying Pathological Huntingtin Exon1 Aggregation." Mol Cell **70**(4): 588-601 e586.
55. Pietrosemoli, N., R. Pancsa and P. Tompa (2013). "Structural disorder provides increased adaptability for vesicle trafficking pathways." PLoS Comput Biol **9**(7): e1003144.
56. Reichheld, S. E., L. D. Muiznieks, F. W. Keeley and S. Sharpe (2017). "Direct observation of structure and dynamics during phase separation of an elastomeric protein." Proc Natl Acad Sci U S A **114**(22): E4408-E4415.
57. Scher-Zagier, J. K. and A. E. Carlsson (2016). "Local Turgor Pressure Reduction via Channel Clustering." Biophys J **111**(12): 2747-2756.
58. Skruzny, M., T. Brach, R. Ciuffa, S. Rybina, M. Wachsmuth and M. Kaksonen (2012). "Molecular basis for coupling the plasma membrane to the actin cytoskeleton during clathrin-mediated endocytosis." Proc Natl Acad Sci U S A **109**(38): E2533-2542.
59. Skruzny, M., A. Desfosses, S. Prinz, S. O. Dodonova, A. Gieras, C. Uetrecht, A. J. Jakobi, M. Abella, W. J. H. Hagen, J. Schulz, R. Meijers, V. Rybin, J. A. G. Briggs, C. Sachse and M. Kaksonen (2015). "An Organized Co-assembly of Clathrin Adaptors Is Essential for Endocytosis." Developmental Cell **33**(2): 150-162.
60. Snead, W. T., C. C. Hayden, A. K. Gadok, C. Zhao, E. M. Lafer, P. Rangamani and J. C. Stachowiak (2017). "Membrane fission by protein crowding." Proc Natl Acad Sci U S A **114**(16): E3258-E3267.
61. Sochacki, K. A., A. M. Dickey, M. P. Strub and J. W. Taraska (2017). "Endocytic proteins are partitioned at the edge of the clathrin lattice in mammalian cells." Nat Cell Biol **19**(4): 352-361.
62. Style, R. W., T. Q. Sai, N. Fanelli, M. Ijavi, K. Smith-Mannschott, Q. Xu, L. A. Wilen and E. R. Dufresne (2018). "Liquid-Liquid Phase Separation in an Elastic Network." Physical Review X **8**(1).
63. Tallinen, T., J. Chung, F. Rousseau, N. Girard, J. Lefèvre and L. Mahadevan (2016). "On the growth and form of cortical convolutions." Nature Physics **12**: 588–593.
64. Tang, H. Y., J. Xu and M. Cai (2000). "Pan1p, End3p, and S1a1p, three yeast proteins required for normal cortical actin cytoskeleton organization, associate with each other and play essential roles in cell wall morphogenesis." Mol Cell Biol **20**(1): 12-25.
65. Thompson, D. A. W. (1917). On growth and form. Cambridge Eng., University press.
66. Toombs, J. A., B. R. McCarty and E. D. Ross (2009). "Compositional Determinants of Prion Formation in Yeast." Molecular and Cellular Biology **30**(1): 319-332.
67. Updike, D. L., S. J. Hachey, J. Kreher and S. Strome (2011). "P granules extend the nuclear pore complex environment in the C. elegans germ line." J Cell Biol **192**(6): 939-948.
68. Wang, J., J. M. Choi, A. S. Holehouse, H. O. Lee, X. Zhang, M. Jahnel, S. Maharana, R. Lemaitre, A. Pozniakovsky, D. Drechsel, I. Poser, R. V. Pappu, S. Alberti and A. A. Hyman (2018). "A Molecular Grammar Governing the Driving Forces for Phase Separation of Prion-like RNA Binding Proteins." Cell.
69. Warren, D. T., P. D. Andrews, C. W. Gourlay and K. R. Ayscough (2002). "Sla1p couples the yeast endocytic machinery to proteins regulating actin dynamics." J Cell Sci **115**(Pt 8): 1703-1715.
70. Wei, M.-T., S. Elbaum-Garfinkle, A. S. Holehouse, C. C.-H. Chen, M. Feric, C. B. Arnold, R. D. Priestley, R. V. Pappu and C. P. Brangwynne (2017). "Phase behaviour of disordered proteins underlying low density and high permeability of liquid organelles." NATURE CHEMISTRY.
71. Weirich, K. L., S. Banerjee, K. Dasbiswas, T. A. Witten, S. Vaikuntanathan and M. L. Gardel (2017). "Liquid behavior of cross-linked actin bundles." Proc Natl Acad Sci U S A **114**(9): 2131-2136.
72. Wu, F. and P. J. Yao (2009). "Clathrin-mediated endocytosis and Alzheimer's disease: an update." Ageing Res Rev **8**(3): 147-149.

857 **73.** Xi, K., T. Byrnes and H. Saito (2017). "Fingering instabilities and pattern formation in a two-component dipolar
858 Bose-Einstein condensate." arXiv **1704.04949v1**
859 74. Youn, J. Y., H. Friesen, T. Kishimoto, W. M. Henne, C. F. Kurat, W. Ye, D. F. Ceccarelli, F. Sicheri, S. D.
860 Kohlwein, H. T. McMahon and B. J. Andrews (2010). "Dissecting BAR domain function in the yeast
861 Amphiphysins Rvs161 and Rvs167 during endocytosis." Mol Biol Cell **21**(17): 3054-3069.
862 75. Yu, H. and K. Schulten (2013). "Membrane sculpting by F-BAR domains studied by molecular dynamics
863 simulations." PLoS Comput Biol **9**(1): e1002892.
864